

Photorefractive Effect in Ferroelectric Liquid Crystals

Takeo SASAKI and Yumiko NAKA

OPTICAL REVIEW Vol. 21, No. 2 (2014)

Photorefractive Effect in Ferroelectric Liquid Crystals

Takeo SASAKI and Yumiko NAKA

Department of Chemistry, Faculty of Science, Tokyo University of Science, Shinjuku, Tokyo 162-8601, Japan

(Received October 29, 2013; Accepted December 29, 2013)

In this paper, we review recent progress of research on the photorefractive effect of ferroelectric liquid crystals. The photorefractive effect is a phenomenon that forms a dynamic hologram in a material. The interference of two laser beams in a photorefractive material establishes a refractive index grating. This phenomenon is applicable to a wide range of devices related to diffraction optics including 3D displays, optical amplification, optical tomography, novelty filters, and phase conjugate wave generators. Ferroelectric liquid crystals are considered as a candidate for practical photorefractive materials. A refractive index grating formation time of 8–10 ms and a large gain coefficient are easily obtained in photorefractive ferroelectric liquid crystals. © 2014 The Japan Society of Applied Physics

Keywords: photorefractive effect, organic compounds, ferroelectric liquid crystals, two beam coupling, dynamic hologram

1. Introduction

The photorefractive effect is a phenomenon that can result in the formation of holographic images within a material. It provides the potential to realize dynamic holograms by recording holograms as a change in the refractive index of a medium.^{1,2)} The photorefractive effect permits two-beam coupling and can be used to coherently amplify signal beams; therefore, it has the potential to be used in a wide range of optical technologies as a transistor for electrical circuits. Optically transparent materials that have both photovoltaic and electro-optic effects can exhibit the photorefractive effect. Many photorefractive materials have been developed, such as inorganic ferroelectric photoconductive crystals, organic crystals, photoconductive nonlinear optical organic polymers, amorphous organic photoconductive materials, photoconductive amphiphilic compounds and photoconductive liquid crystals (LCs).^{3–5)} Since 1994, organic materials have attracted significant interest because they exhibit large photorefractivity and a shorter response time.⁶⁾ The photorefractive effect induces a change in the refractive index by a mechanism that involves both photovoltaic and electro-optic effects (Fig. 1). When two laser beams interfere in an organic photorefractive material, charge generation occurs at the bright positions of the interference fringes. The generated charges diffuse or drift within the material. The mobilities of positive and negative charges are different in most organic materials, so that a charge separated state is formed. The charge with higher mobility diffuses over a longer distance than that with lower mobility; therefore, while the low mobility charge stays in the light areas, the high mobility charge moves to the dark areas. The light and dark positions of the interference fringes are thus charged with opposite polarities, and an internal electric field (space charge field) appears in the area between the light and dark positions. The refractive index of the area between the light and dark positions is changed through the electro-optic effect. Thus, a refractive index grating (hologram) is formed. A high electric field of 10–50 V/ μm is usually applied to a polymer film, aside from the

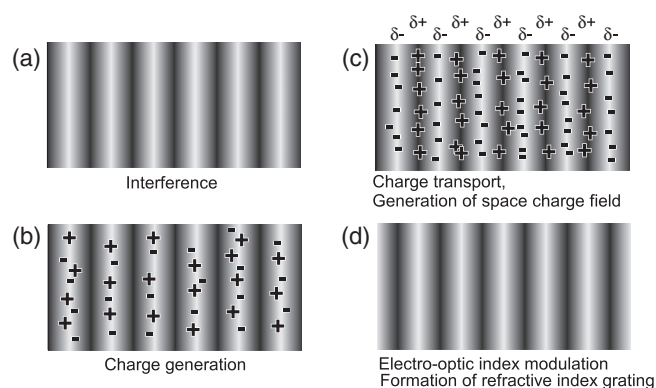


Fig. 1. Schematic illustration of the mechanism of the photorefractive effect. (a) Two laser beams interfere in the photorefractive material, (b) charge generation occurs in the light areas of the interference fringes, (c) electrons are trapped at the trap sites in the light areas, holes migrate by diffusion or drift in the presence of an external electric field and generate an internal electric field between the light and dark positions, and (d) the refractive index of the corresponding area is altered by the internal electric field that is generated.

internal electric field, to obtain photorefractivity in polymer materials. The polymer material is typically 100 μm thick, so that the voltage necessary to achieve photorefractivity is 1–5 kV, which is almost comparable to the breakdown voltage of the polymer film. This electric field is necessary to increase the charge generation efficiency. One material class that exhibits high photorefractivity is glassy photoconductive polymers doped with high concentrations of D- π -A chromophores, in which the donor and acceptor groups are attached to a π -conjugate system.^{3–7)} A multiplex hologram has been demonstrated using a photorefractive polymer film during the development of a 3D display^{8,9)} and clear 3D images were recorded in the film. However, the slow response (ca. 100 ms) and the high electric field (30–50 V/ μm) required to activate the photorefractive effect in polymer materials require improvement. The photorefractive

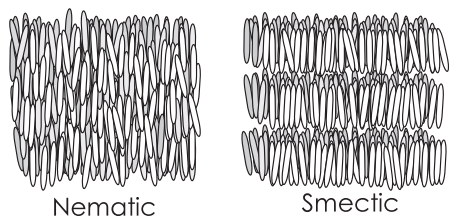


Fig. 2. Structures of the nematic and smectic phases.

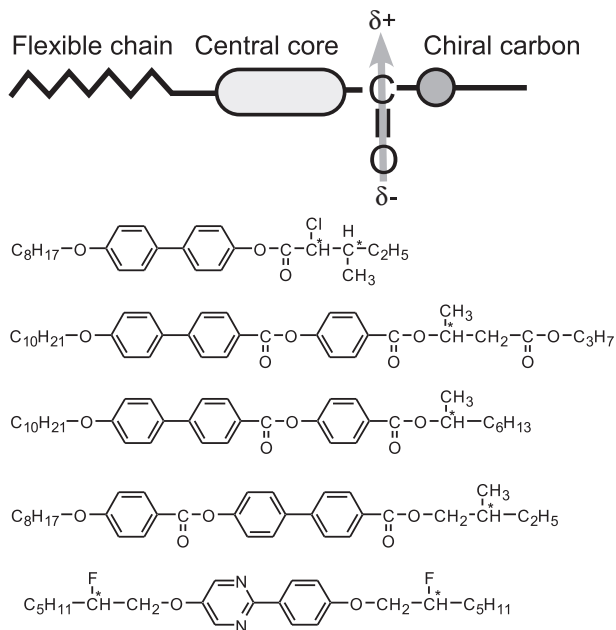


Fig. 3. Molecular structures of FLCs.

effect of LCs has also been investigated.¹⁰ LCs are basically liquid, so they can be easily driven by a low electric field. LCs are classified into several groups, the most well known of which are nematic and smectic LCs (Fig. 2). Nematic LCs are used in liquid crystal displays (LCDs), whereas smectic LCs are very viscous and are thus seldom utilized in practical applications. Nematic LCs were first used as a photorefractive LC and large photorefractivity was obtained with the application of an electric field of only a few volts per micrometer.¹¹ The photorefractive effect has been reported in surface-stabilized ferroelectric liquid crystals (SS-FLCs) doped with a photoconductive compound.^{12,13} Ferroelectric liquid crystals (FLCs) belong to the class of smectic LCs that have a layered structure.^{14,15} The molecular structure of a typical FLC contains a chiral unit, a carbonyl group, a central core that has a rigid rod-like structure such as biphenyl or phenylpyrimidine, phenylbenzoate, and a flexible alkyl chain (Fig. 3). Thus, the dipole moment of an FLC molecule is perpendicular to the molecular long axis. FLCs exhibit a chiral smectic C phase (SmC^*) that possesses a helical structure. It should be noted here that to observe ferroelectricity in these materials, the FLCs must be formed into thin films.¹⁴ The thickness of the film must be a few micrometers. When an FLC is

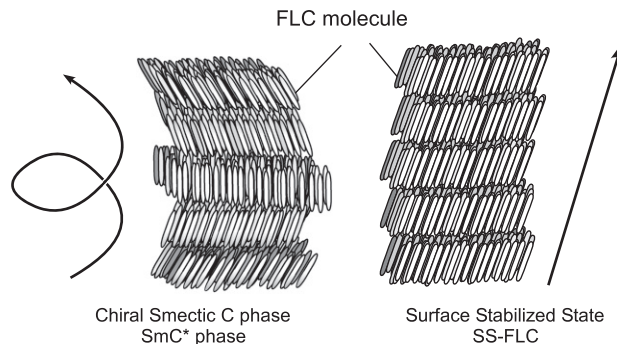
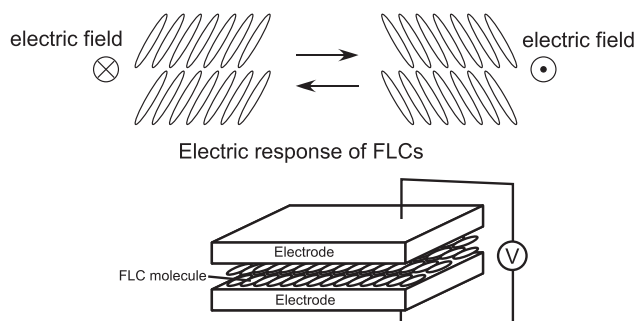
Fig. 4. Structures of the SmC phase and the SS-state of the SmC phase (SS-FLC).

Fig. 5. Electro-optical switching in the SS-state of FLCs.

sandwiched between glass plates to form a film a few micrometers thick, the helical structure of the SmC^* phase uncoils and a surface-stabilized state (SS-state) is formed in which spontaneous polarization (P_s) appears (Fig. 4). For display applications, the thickness of the film is usually $2\ \mu\text{m}$. In such thin films, FLC molecules can align in only two directions, which is the SS-state, and the alignment direction of the FLC molecules changes according to the direction of the spontaneous polarization (Fig. 5). When an alternating electric field is applied to the SS-FLC, the FLC molecules show a continuous switching motion. The electrical switching response time of FLCs is typically shorter than 1 ms. The direction of the spontaneous polarization is governed by the applied electric field, which gives rise to a change in properties according to the direction of polarization. Thus, when an internal electric field is created in an SS-FLC material, the direction of spontaneous polarization is changed by the field. Figure 6 shows a schematic illustration of the mechanism of the photorefractive effect in FLCs. When laser beams interfere in a mixture of an FLC and a photoconductive compound, charge separation occurs between the light and dark positions and internal electric fields are produced. The internal electric field alters the direction of spontaneous polarization in the area between the light and dark positions of the interference fringes, which induces a periodic change in the orientation of the FLC molecules. This is different from the processes that occur in other organic photorefractive materials, in that the

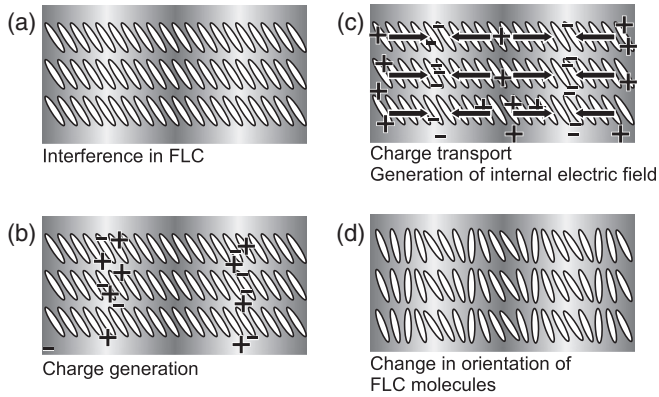


Fig. 6. Schematic illustration of the mechanism of the photorefractive effect in FLCs. (a) Two laser beams interfere in the SS-state of the FLC/photoconductive compound mixture; (b) charge generation occurs in the light areas of the interference fringes; (c) electrons are trapped at the trap sites in the light areas, holes migrate by diffusion or drift in the presence of an external electric field to generate an internal electric field between the light and dark positions, and (d) the orientation of the spontaneous polarization vector (i.e., orientation of mesogens in the FLCs) is altered by the internal electric field.

molecular dipole rather than the bulk polarization responds to the internal electric field. The switching of FLC molecules is due to the response of bulk polarization and is thus extremely fast.

2. Characteristics of the Photorefractive Effect

A change in the refractive index via the photorefractive effect occurs in the areas between the light and dark positions of the interference fringes, so that the phase of the resulting index grating is shifted from the interference fringes. A characteristic of the photorefractive effect is that the phase of the refractive index grating is $\pi/2$ -shifted from the interference fringes under conditions where one of the photogenerated charges does not move from the light position. When the material is photochemically active and is not photorefractive, then a photochemical reaction occurs at the light areas, and a refractive index grating with the same phase as that of the interference fringes is formed [Fig. 7(a)]. The interfering laser beams are diffracted by this grating; however, when the intensities of the interfering beams are equal, the apparent transmitted intensities of the laser beams do not change, because the diffraction is symmetric. Beam 1 is diffracted in the direction of beam 2 and beam 2 is diffracted in the direction of beam 1. However, if the material is photorefractive, then the phase of the refractive index grating is shifted from that of the interference fringes, and this affects the propagation of the two beams. Beam 1 is energetically coupled with beam 2 for two laser beams, and consequently, the apparent transmitted intensity of beam 1 increases while that of beam 2 decreases [Fig. 7(b)]. This phenomenon where one beam is amplified by another beam is termed asymmetric energy exchange in a two-beam coupling experiment.^{1,2)} The photorefractivity of a material

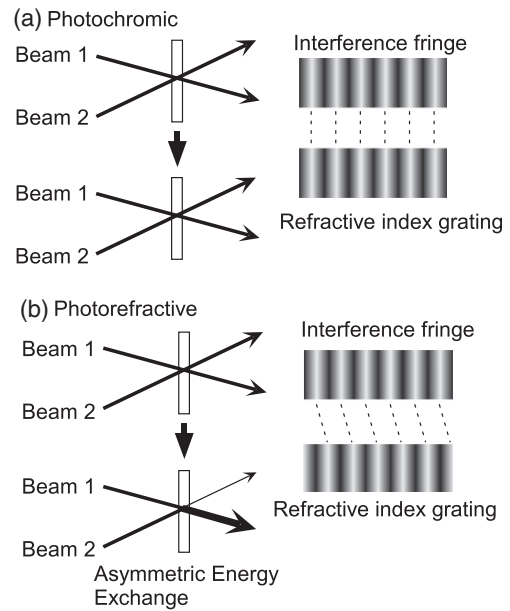


Fig. 7. (a) Photochromic grating and (b) photorefractive grating.

is confirmed by the occurrence of this asymmetric energy exchange, which has the potential for a vast variety of optical applications.

3. Evaluation of Photorefractivity

The photorefractive effect was evaluated using a two-beam coupling method and also with a four-wave mixing experiment. Figure 8(a) shows a schematic illustration of the experimental setup used for the two-beam coupling method. A p-polarized beam from a laser is divided into two beams by a beam splitter and the beams are allowed to interfere within the sample film. An electric field is applied to the sample using a high-voltage supply unit. This external electric field is applied to increase the efficiency of charge generation in the film. The change in the transmitted beam intensity is monitored; if a material is photorefractive, then an asymmetric energy exchange is observed. The magnitude of photorefractivity is evaluated with respect to a parameter called the gain coefficient, which is calculated from the change in the transmitted intensity of the laser beams induced through the two-beam coupling. To calculate the two-beam coupling gain coefficient, it must be determined whether the diffraction condition is in the Bragg regime or in the Raman–Nath regime. These diffraction conditions are distinguished by a dimensionless parameter Q .²⁾

$$Q = 2\pi\lambda L/n\Lambda^2, \quad (1)$$

where λ is the wavelength of the laser, L is the interaction path length, n is the refractive index and Λ is the grating spacing. $Q > 1$ is defined as the Bragg regime of optical diffraction. In this regime, multiple scattering is not permitted and only one order of diffraction is produced. Conversely, $Q < 1$ is defined as the Raman–Nath regime of optical diffraction. In this regime, many orders of diffraction can be observed. $Q > 10$ is typically required to guarantee

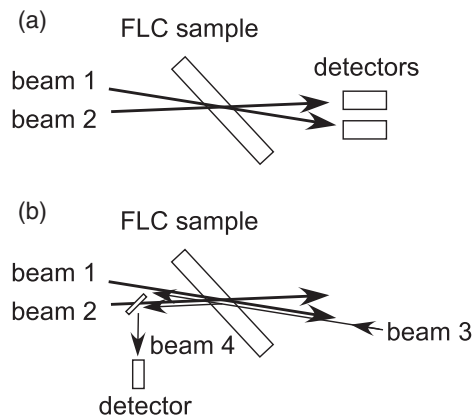


Fig. 8. Schematic illustrations of the experimental setup for the (a) two-beam coupling and (b) four-wave-mixing techniques.

that the diffraction is entirely in the Bragg regime. When the diffraction is in the Bragg regime, the two-beam coupling gain coefficient Γ (cm^{-1}) is defined as:¹⁻³⁾

$$\Gamma = \frac{1}{D} \ln\left(\frac{gm}{1+m-g}\right), \quad (2)$$

where $D = L/\cos(\theta)$ is the interaction path for the signal beam ($L =$ sample thickness, $\theta =$ propagation angle of the signal beam in the sample), g is the ratio of the signal beam intensities behind the sample with and without a pump beam, and m is the ratio of the beam intensities (pump/signal) in front of the sample.

A schematic illustration of the experimental setup used for the four-wave mixing experiment is shown in Fig. 8(b). S-polarized writing beams (beam 1 and beam 2) are allowed to interfere in the sample film and the diffraction of a p-polarized probe beam (beam 3), which counter-propagates to one of the writing beams, is measured (beam 4). The diffracted beam intensity is typically measured as a function of time, applied (external) electric field, and writing beam intensity. The diffraction efficiency is defined as the ratio of the diffracted beam intensity to the probe beam intensity that is transmitted when no grating is present in the sample owing to the writing beams. When the grating is probed, it is important that beam 3 does not affect the grating or interact with the writing beams. This can be ensured by making the probe beam much weaker than the writing beams and by having the probe beam polarized orthogonal to the writing beams.

4. Photorefractive Effect of FLCs

4.1 Two-beam coupling experiments with FLCs

Investigations on the photorefractive effect of FLCs started around 2000.^{12,13)} The photorefractive FLC is a mixture of FLC and photoconductive compounds. Details of the photorefractivity in FLC materials have since been further investigated by Sasaki and coworkers and Golemme and coworkers.¹⁶⁻²³⁾ The photorefractive effect in a mixture of an FLC and a photoconductive compound was measured in a two-beam coupling experiment with a 488 nm Ar^+ laser.

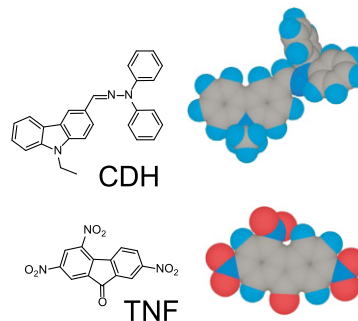


Fig. 9. (Color online) Structures of the photoconductive compound CDH and the sensitizer TNF.

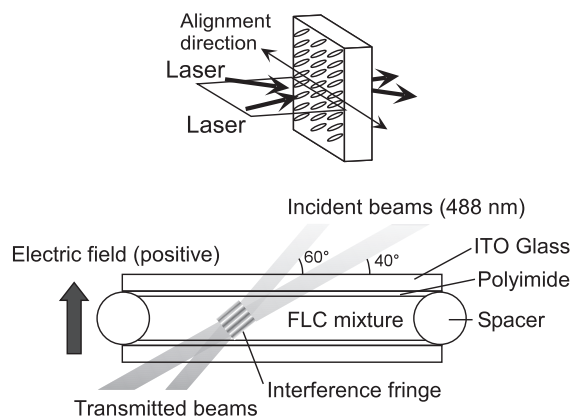


Fig. 10. Laser beam incidence condition and the structure of the LC cell.

The wavelength of the laser is determined according to the photoconductive compounds used in the photorefractive FLC mixture. The structures of the photoconductive compounds used are shown in Fig. 9. A commercially available FLC, SCE8 (Clariant, $\text{SmC}^* 60^\circ\text{C SmA } 80^\circ\text{C N}^* 104^\circ\text{C I}$, spontaneous polarization = 4.5 nC/cm^2), was used in the primary investigations. SCE8 is a mixture of LC compounds and chiral compounds. Carbazole diphenylhydrazone (CDH) was used as a photoconductive compound, and trinitrofluorenone (TNF) was used as a sensitizer. The concentrations of CDH and TNF were 2 and 0.1 wt%, respectively. The samples were injected into a 10- μm -gap glass cell equipped with 1 cm^2 indium tin oxide (ITO) electrodes and a polyimide alignment layer (Fig. 10). Figure 11 shows a typical example of the asymmetric energy exchange observed in the FLC (SCE8)/CDH/TNF sample under an applied DC electric field of $0.1 \text{ V}/\mu\text{m}$.¹⁷⁾ Interference of the divided beams in the sample resulted in increased transmittance of one beam and decreased transmittance of the other. The change in the transmitted intensities of the two beams is completely symmetric, as shown in Fig. 11. This indicates that the phase of the refractive index grating is shifted from that of the interference fringes. The grating formation was within the Bragg diffraction regime and no higher order diffraction was observed under the experimental conditions.

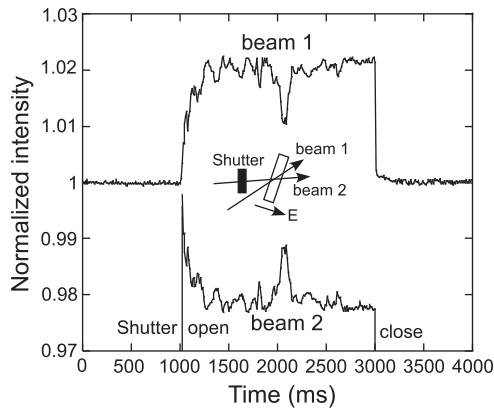


Fig. 11. Typical example of asymmetric energy exchange observed in an FLC (SCE8) mixed with 2 wt % CDH and 0.1 wt % TNF with an electric field of $+0.3 \text{ V}/\mu\text{m}$ applied to the sample.

The temperature dependence of the gain coefficient of the FLC (SCE8) doped with 2 wt % CDH and 0.1 wt % TNF is shown in Fig. 12(a). Asymmetric energy exchange was observed only at temperatures below 46°C in this sample. The spontaneous polarization of an identical sample is plotted as a function of temperature in Fig. 12(b). Similarly, the spontaneous polarization vanished when the temperature was raised above 46°C . Thus, asymmetric energy exchange was observed only in the temperature range in which the sample exhibits ferroelectric properties, i.e., the SmC^* phase. The molecular dipole moment of the FLCs is small and the dipole moment is aligned perpendicular to the molecular axis; therefore, large changes in the orientation of the molecular axis cannot be induced by an internal electric field in the SmA or N^* phases of the FLCs. However, in the SmC^* phase, reorientation associated with spontaneous polarization occurs owing to the internal electric field. The spontaneous polarization also causes the orientation of FLC molecules in the corresponding area to change accordingly. A maximum resolution of $0.8 \mu\text{m}$ was obtained for this sample.¹⁷⁾

4.2 Effect of the applied electric field magnitude

For polymeric photorefractive materials, the strength of the externally applied electric field is a very important factor. The external electric field is necessary to sufficiently increase the charge separation efficiency to induce a photorefractive effect; the photorefractivity of the polymer is obtained with only an electric field larger than a few volts per micrometer. The thickness of the polymeric photorefractive material commonly reported is approximately $100 \mu\text{m}$, so the voltage necessary to induce the photorefractive effect is a few kilovolts. In contrast, the photorefractive effect in FLCs can be induced by application of a very weak external electric field. The maximum gain coefficient for the FLC (SCE8) sample was obtained using an electric field strength of only $0.2\text{--}0.4 \text{ V}/\mu\text{m}$. The thickness of the FLC sample is typically $10 \mu\text{m}$, so the voltage necessary to induce the photorefractive effect is only a few volts. The dependence of the gain coefficient of a

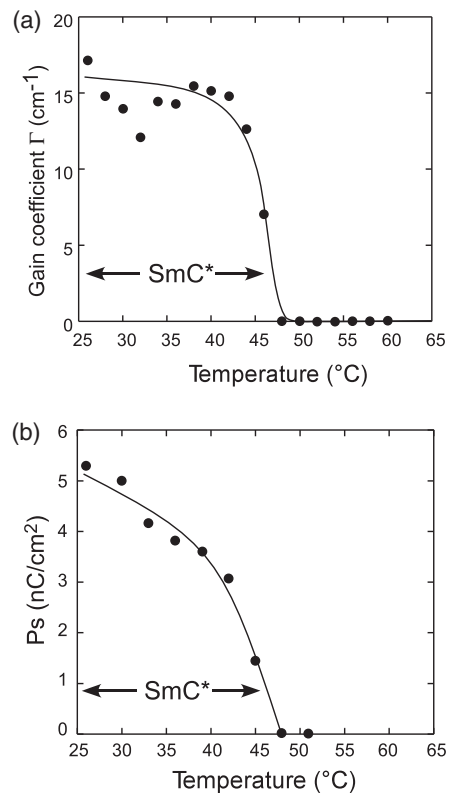


Fig. 12. Temperature dependence of the (a) gain coefficient and (b) spontaneous polarization of an FLC (SCE8) mixed with 2 wt % CDH and 0.1 wt % TNF. For two-beam coupling experiments, an electric field of $0.1 \text{ V}/\mu\text{m}$ was applied to the sample.

mixture of FLC (SCE8)/CDH/TNF on the strength of the electric field is shown in Fig. 13. The gain coefficient of SCE8 doped with $0.5\text{--}1 \text{ wt } \%$ CDH increased with the strength of the external electric field. However, the gain coefficient of SCE8 doped with 2 wt % CDH decreased when the external electric field exceeded $0.4 \text{ V}/\mu\text{m}$. The same tendency was also observed for another commercially available FLC; M4851/050 (Clariant, SmC^* 65°C SmA 70°C N^* 74°C I , spontaneous polarization = $14 \text{ nC}/\text{cm}^2$). The formation of an orientational grating is enhanced when the external electric field is increased from 0 to $0.2 \text{ V}/\mu\text{m}$ as a result of the induced charge separation. However, when the external electric field exceeded $0.2 \text{ V}/\mu\text{m}$, a number of zigzag defects appeared in the SS-state. These defects cause light scattering and result in a decrease of the gain coefficient. The gain coefficient of FLC materials reported around 2003 (Fig. 13)¹⁶⁾ was much smaller than that of polymer materials.

4.3 Refractive index grating formation time

The formation of a refractive index grating involves charge separation and reorientation. The index grating formation time (response time of the photorefractive effect) is affected by these two processes, and both may be rate-determining steps. The refractive index grating formation times for the commercially available FLCs (SCE8 and M4851/050) examined were determined based on the

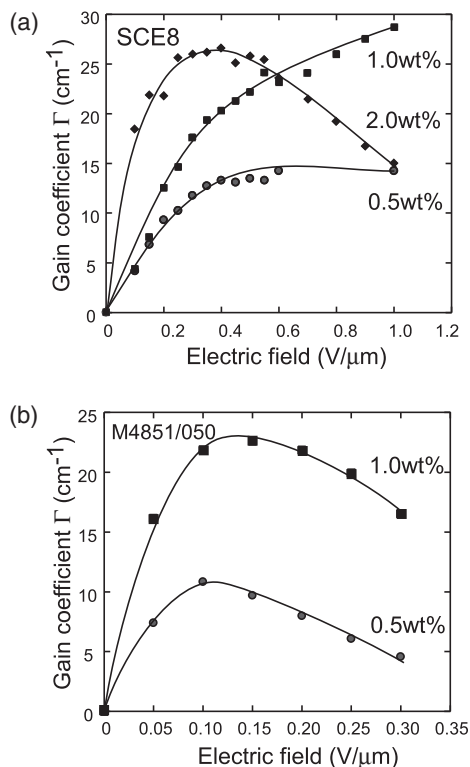


Fig. 13. Electric field dependence of the gain coefficient for SCE8 and M4851/050 mixed with several concentrations of CDH and 0.1 wt % TNF in a 10- μm -gap cell measured at 30 °C.

simplest single-carrier model of photorefractivity,^{1,2)} wherein the gain transient is exponential. The rising signal of the diffracted beam was fitted using a single exponential function:

$$\gamma(t) - 1 = (\gamma - 1)[1 - \exp(-t/\tau)]^2, \quad (3)$$

where $\gamma(t)$ represents the transmitted beam intensity at time t divided by the initial intensity [$\gamma(t) = I(t)/I_0$], and τ is the formation time. The grating formation time in SCE8/CDH/TNF is plotted as a function of the external electric field strength in Fig. 14. The grating formation time decreased with increasing electric field strength owing to the increased efficiency of charge generation. The formation time was shorter at higher temperatures, which corresponded to a decrease in the viscosity of the FLC with increasing temperature. The formation time for SCE8 was 20 ms at 30 °C. The response time of FLC materials is thus faster than those of polymer materials, in which the typical response time is reported to be around 100 ms.^{3,4)}

4.4 Photorefractive effect in FLC mixtures containing photoconductive chiral compounds

4.4.1 Photoconductive chiral dopants

Compared with nematic LCs, FLCs are more crystalline than liquid, so the preparation of fine FLC films requires several sophisticated techniques. It is very difficult to obtain a uniformly aligned, defect-free SS-FLC using a single FLC compound. Consequently, mixtures of several LC compounds are usually used to obtain fine SS-FLC films. The

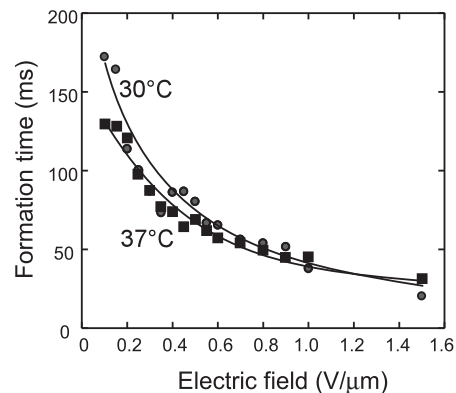


Fig. 14. Electric field dependence of the index grating formation time. FLC (SCE8) mixed with 2 wt % CDH and 0.1 wt % TNF in a two-beam coupling experiment. ●: measured at 30 °C ($T/T_{\text{SmC}^*-\text{SmA}} = 0.95$); ■: measured at 36 °C ($T/T_{\text{SmC}^*-\text{SmA}} = 0.97$).

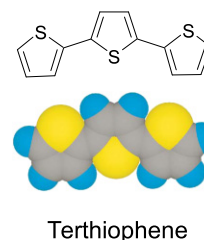


Fig. 15. (Color online) Structure of terthiophene.

FLC mixtures are composed of a base LC, which is a mixture of several LC compounds, and a chiral compound. The chiral compound introduces a helical structure to the LC phase through supramolecular interactions. Utilizing an FLC as a photorefractive material requires the addition of photoconductive compounds to the FLC. However, the introduction of such non-LC compounds to the FLC often hinders the formation of a uniformly aligned SS-state. Thus, appropriate design of the photoconductive compounds is crucial. The photorefractive effect of FLC mixtures containing photoconductive chiral dopants has been investigated.²²⁾ Terthiophene was chosen as a photoconductive chromophore because it is a well known semiconductor compound and has a rod-like structure (Fig. 15) which will increase the solubility into the rod-like structured LC material. The structures of the LC compounds, the electron acceptor TNF, and photoconductive chiral compounds are shown in Fig. 16.

The mixing ratio of 8PP8 and 8PP10 was set at 1 : 1 because a 1 : 1 mixture exhibits the SmC phase over the widest temperature range. Hereafter, the 1 : 1 mixture of 8PP8 and 8PP10 is referred to as the base LC. The concentration of TNF was 0.1 wt %. Four photoconductive chiral compounds with the terthiophene chromophore (3T-2MB, 3T-2OC, 3T-OXO, and 3T-CF3) were synthesized. The base LC, TNF, and a photoconductive chiral compound were dissolved in dichloroethane, and the solvent was

evaporated. The mixture was then dried under vacuum at room temperature for one week. The samples were subsequently injected into a 10 μm gap glass measurement cell equipped with 1 cm^2 ITO electrodes and a polyimide alignment layer. The base LC was mixed with the photoconductive chiral dopant and TNF as the electron acceptor. The terthiophene chiral dopants have high miscibility with the phenylpyrimidine-type smectic LCs. The chiral SmC* phase appeared in all mixtures of the base LC with the various chiral dopants. The temperature ranges of the SmC* and chiral nematic (N*) phases were reduced with the concentration of the chiral dopants, whereas that of the SmA phase was widened. The miscibility of 3T-CF3

with the base LC was the lowest among the four chiral dopants, which was considered to be due to the aggregation of 3T-CF3 molecules because the dipole moment of the trifluoromethyl substituted group is large. All the samples exhibited absorption maxima at 394 nm, whereas absorption at 488 nm (wavelength of the laser used) was small. The absorption spectra were not changed when TNF (1.0×10^{-5} mol/L) was added to the solution. The small absorption at the laser wavelength is advantageous to minimize the optical loss.

Photocurrents in mixtures of the base LC, photoconductive chiral dopants and TNF were measured. Figure 17 shows that these samples were good insulators in the dark. Photocurrents were observed when the samples were irradiated with the 488 nm laser. The magnitudes of the photocurrents were slightly different for the four samples. The only difference in the molecular structures of these compounds is the chiral substituent; therefore, the difference in the photocurrent cannot be attributed to the difference in the molecular structure. It is considered that the miscibility of the photoconductive chiral compound with the LC and the homogeneity of the LC phase affected the magnitude of the photocurrent.

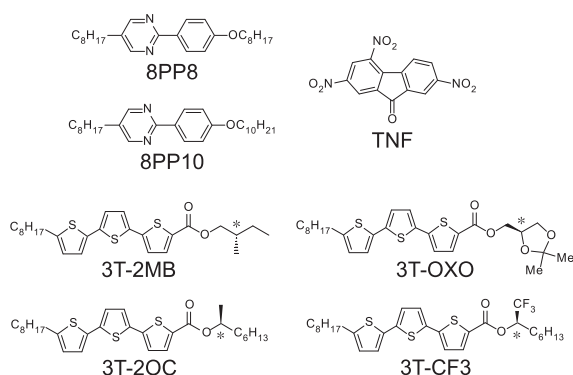


Fig. 16. Structures of the smectic LCs (8PP8 and 8PP10), photoconductive chiral dopants (3T-2MB, 3T-2OC, 3T-OXO, and 3T-CF3) and the sensitizer TNF.

4.4.2 Two-beam coupling experiment with photoconductive FLC mixtures

The photorefractive effect was measured in a two-beam coupling experiment.²²⁾ A linearly p-polarized beam from an Ar⁺ laser (488 nm, continuous wave) was divided in two by a beam splitter and the beams were then allowed to interfere

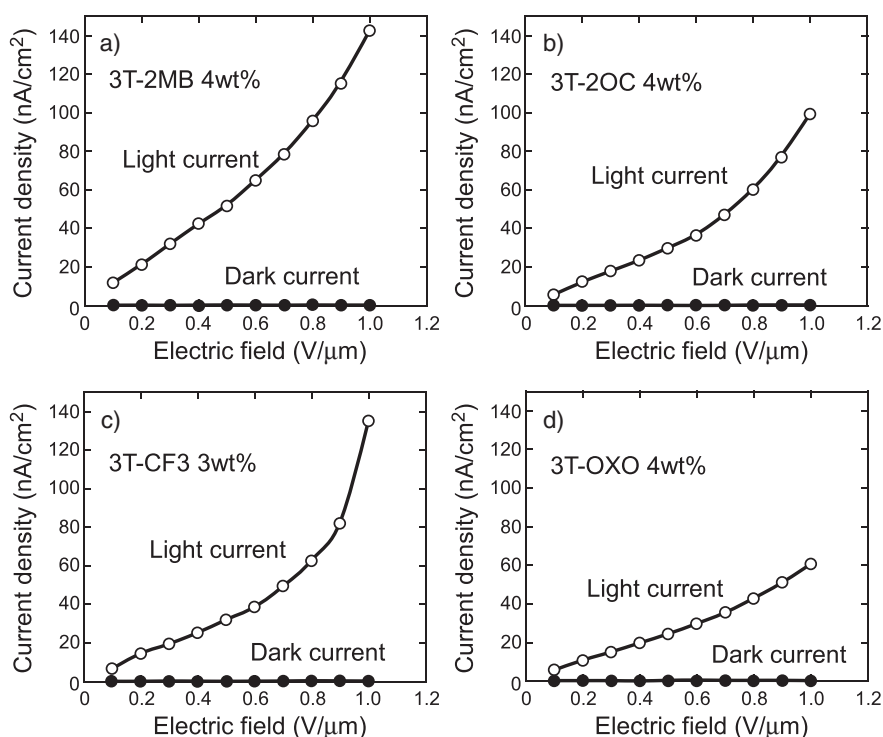


Fig. 17. Magnitudes of light-current and dark-current for mixtures of the base LC, photoconductive chiral compound, and TNF measured in a 10- μm -gap LC cell as a function of the external electric field. An electric field of 0.1 $\text{V}/\mu\text{m}$ was applied. A 488 nm Ar⁺ laser ($10 \text{ mW}/\text{cm}^2$, 1 mm diameter) was used as the irradiation source.

in the sample film. The laser intensity was 2.5 mW for each beam (1 mm diameter). The incident angles of the beams to the glass plane were 30 and 50°. The interval between interference fringes was 1.87 μm . Figure 18 shows typical examples of the asymmetric energy exchange observed for a mixture of the base LC, 3T-2MB, and TNF at 30 °C with application of an electric field in the range of 0.2–0.4 V/ μm . Interference of the divided beams in the sample resulted in increased transmittance of one of the beams and decreased transmittance of the other beam. These transmittance characteristics were reversed when the polarity of the applied electric field was reversed. Asymmetric energy exchange was only observed when an electric field was applied, which indicates that the beam coupling was not caused by a thermal grating. The magnitude of the gain coefficient increased with the concentration of 3T-2MB. Calculating the two-beam coupling gain coefficient required

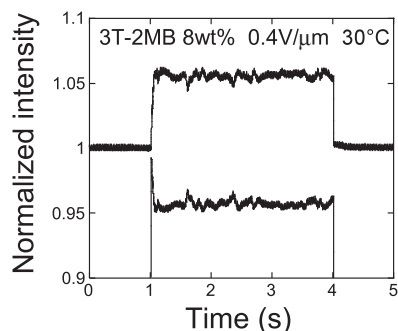


Fig. 18. Typical results of two-beam coupling experiments for mixtures of the base LC, 3T-2MB, and TNF measured at 30 °C.

correct identification of the diffraction condition. The difference in the gain coefficients for mixtures of the base LC, photoconductive chiral dopants (3T-2MB, 3T-2OC, 3T-OXO, and 3T-CF3), and TNF was investigated. All the samples formed finely aligned SS-states in 10- μm -gap cells with an LX-1400 polyimide alignment layer and exhibited clear photorefractivity in the ferroelectric phase. Asymmetric energy exchange was observed only in the temperature range in which the sample exhibits ferroelectric properties, i.e., the SmC* phase. The gain coefficients of the samples are plotted as a function of the external electric field magnitude in Fig. 19. The gain coefficient increased with the strength of the external electric field in the range of 0.2–0.6 V/ μm , then decreased with a further increase in the strength of the external electric field. The gain coefficients increased with the concentrations of the photoconductive chiral dopants. This may be due to an increase in the charge carrier density in the FLC medium and an increase in the magnitude of Ps. All the samples exhibited relatively large photorefractivity. A gain coefficient higher than 100 cm^{-1} was obtained for the 6 wt% 3T-2OC sample with the application of only 0.2 V/ μm . This means that a voltage of only 2 V is required to obtain a gain coefficient of 100 cm^{-1} in a 10 μm FLC sample. Previously reported gain coefficients of only 50–60 cm^{-1} were obtained for FLCs with application of 1 V/ μm . A gain coefficient higher than 100 cm^{-1} was also obtained for the 3T-2MB sample at an applied electric field of 0.5 V/ μm .

To obtain photorefractivity in polymer materials, application of a high electric field of 10–50 V/ μm is typically required. The small electric field necessary to activate the photorefractive effect in FLCs is thus a significant advantage

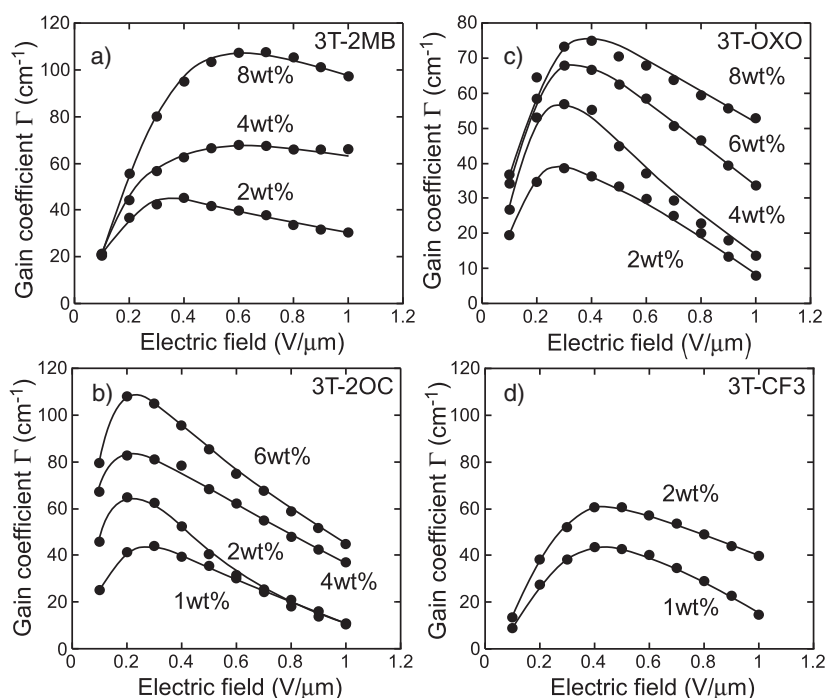


Fig. 19. Electric field dependence of the gain coefficients for mixtures of the base LC, various concentrations of the photoconductive chiral compounds, and TNF: (a) 3T-2MB, (b) 3T-2OC, (c) 3T-OXO, and (d) 3T-CF3.

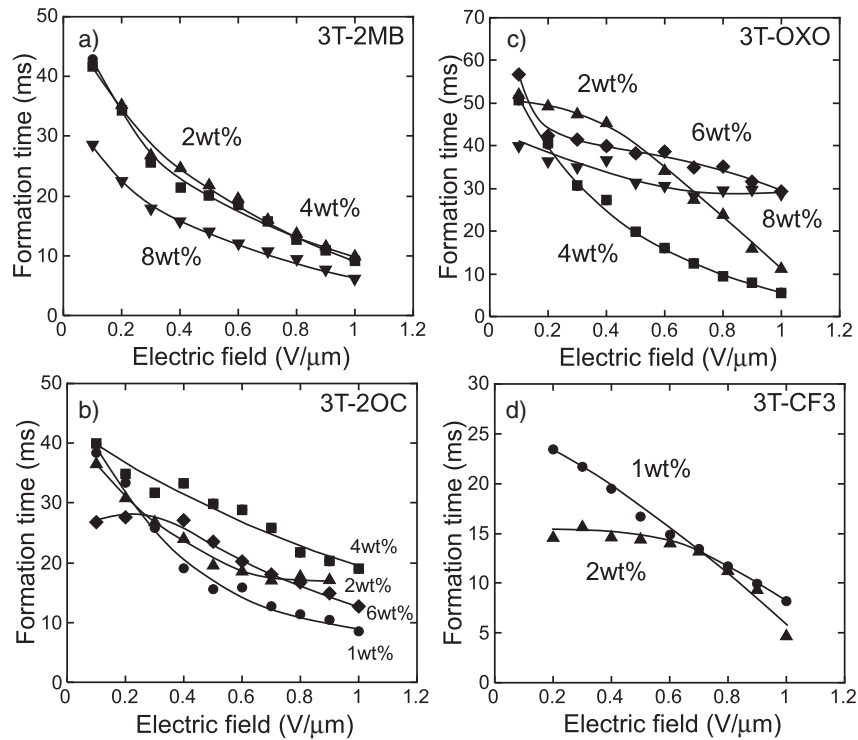


Fig. 20. Electric field dependence of the index grating formation times for mixtures of the base LC, various concentrations of the photoconductive chiral compounds, and TNF measured at 30 °C: (a) 3T-2MB, (b) 3T-2OC, (c) 3T-OXO, and (d) 3T-CF3.

for use in photorefractive devices. The miscibility of 3T-CF3 with the base LC was low and it could only be mixed with the base LC at concentrations of less than 2 wt%. The grating formation times for the mixtures of base LC, photoconductive chiral dopants, and TNF are plotted as a function of the external electric field strength in Fig. 20. The grating formation time decreased with increasing electric field strength owing to the increased efficiency of charge generation. The shortest formation times obtained were 5–8 ms at 1 V/μm for all the chiral photoconductive dopants. The 3T-CF3 sample had the fastest response, owing to the larger polarity of 3T-CF3.

4.4.3 Photorefractive effect in ternary mixture of SmC LC doped with a photoconductive chiral compound

The photorefractive effect of the FLC mixture shown in Fig. 21 was investigated.²³⁾ A typical example of the two-beam coupling experiment for the ternary mixture of base LC, 3T-2MB, and TNF measured at 30 °C is shown in Fig. 22. The ternary mixture base LC exhibited higher transparency than a binary mixture base LC, and very large energy coupling was observed in the material. Over 40% of the intensity of one of the interfering laser beams was transferred to the other beam within an FLC film that was only 10 μm thick. The gain coefficients of the samples were measured as a function of the applied electric field strength [Fig. 23(a)] and were higher than 800 cm⁻¹ for the 10 wt% 3T-2MB sample with application of only 1 V/μm. This gain coefficient is eight times higher than those of FLCs described in Sect. 4.4.2. It is considered that the higher

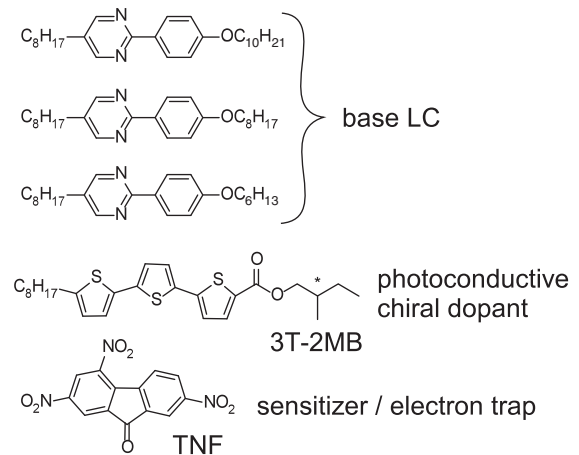


Fig. 21. Photorefractive FLC mixture containing ternary mixture of smectic LCs.

transparency of the ternary LC mixture contributes to the high gain coefficient. In addition, the small electric field required to activate the photorefractive effect in FLCs is advantageous for photorefractive devices. The response time decreased with increasing electric field strength owing to the increased charge separation efficiency [Fig. 23(b)]. The shortest formation time obtained was 8 ms for an external electric field of 1.5 V/μm. The large gain and fast response are advantageous for the realization of optical devices such as real-time image amplifiers and accurate measurement devices.

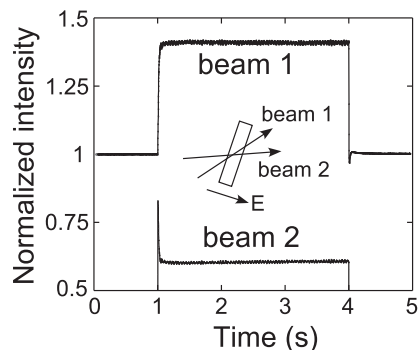


Fig. 22. Typical results of two-beam coupling experiments for a ternary mixture base LC, 3T-2MB, and TNF measured at 30 °C.

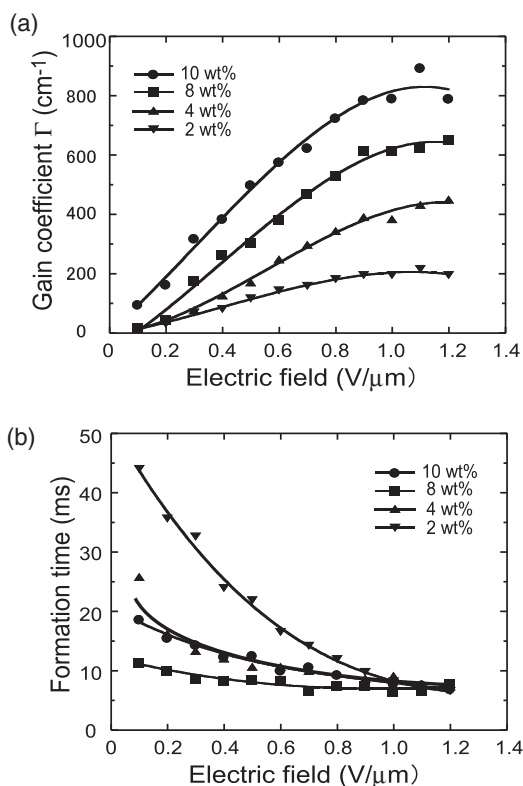


Fig. 23. (a) Electric field dependence of the gain coefficients for mixtures of base LC, 3T-2MB (2–10 wt%), and TNF (0.1 wt%) measured at 30 °C. (b) Refractive index grating formation times (response time) for mixtures of base LC, 3T-2MB (2–10 wt%), and TNF (0.1 wt%) measured at 30 °C.

4.4.4 Formation of dynamic holograms in FLC mixtures

The formation of a dynamic hologram was demonstrated.²³⁾ A computer-generated animation was displayed on a spatial light modulator (SLM). A 488 nm beam from a diode-pumped solid-state (DPSS) laser was irradiated onto the SLM and the reflected beam was incident on the FLC sample. A reference beam was allowed to interfere with the beam from the SLM in the FLC sample. The refractive index grating formed was in the Raman–Nath regime, in which multiple scattering is allowed. A 633 nm beam from a

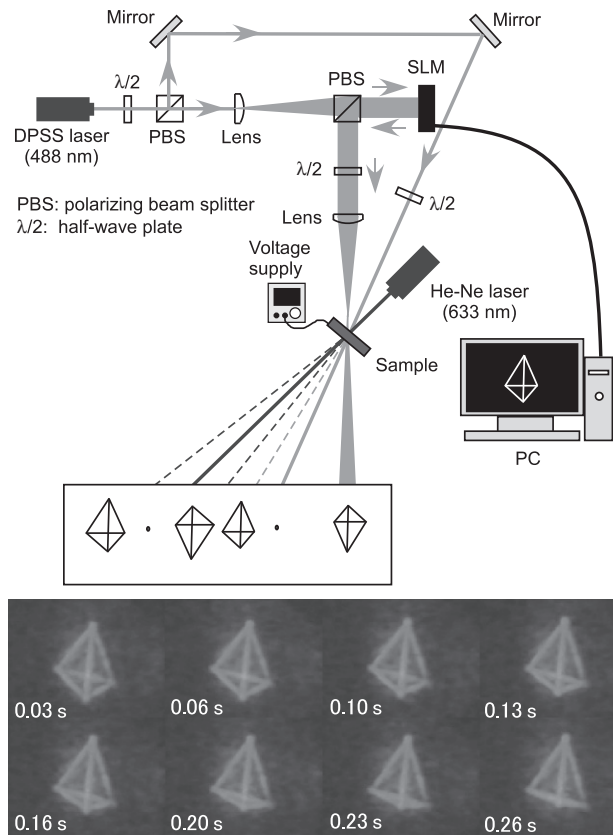


Fig. 24. Dynamic hologram formation experiment on an FLC sample. A computer-generated animation was displayed on the SLM. The SLM modulated the object beam (488 nm), which was irradiated on the FLC sample and allowed to interfere with the reference beam. The readout beam (633 nm) was irradiated on the FLC and diffraction was observed.

He–Ne laser was irradiated on the FLC sample and the diffraction was observed. A moving image of the animation on the computer monitor was observed in the diffracted beam (Fig. 24). No image retention was observed, which means that the hologram image (refractive index grating) formed in the FLC was rewritten with sufficient speed to project a smooth reproduction of a holographic movie.

5. Conclusions

The reorientational photorefractive effect based on the response of bulk polarization was observed in dye-doped FLC mixtures. Photorefractivity was observed only in the ferroelectric phase of these samples and the refractive index formation time was shorter than that of nematic LCs. The response time was of sub-millisecond order and is dominated by the formation of an internal electric field. These results indicate that the mechanism responsible for the formation of a refractive index grating in FLCs is different from that for non-ferroelectric materials and is clearly related to the ferroelectric properties of the material. The photorefractivity of FLCs was strongly affected by the properties of the FLCs. Besides properties such as spontaneous polarization, viscosity, and phase transition

temperature, the homogeneity of the SS-state was also found to be a major factor. The gain coefficient and refractive index grating formation time (response time) were strongly affected by the homogeneity of the SS-state. Therefore, a highly homogeneous SS-state is necessary to create a photorefractive device.

Acknowledgments

The authors would like to thank the Japan Science and Technology Agency (JST) S-innovation and the Canon Foundation for support.

References

- 1) L. Solymar, J. D. Webb, and A. Grunnet-Jepsen: *The Physics and Applications of Photorefractive Materials* (Oxford University Press, New York, 1996).
- 2) P. Yeh: *Introduction to Photorefractive Nonlinear Optics* (Wiley, New York, 1993).
- 3) W. E. Moerner and S. M. Silence: *Chem. Rev.* **94** (1994) 127.
- 4) O. Ostroverkhova and W. E. Moerner: *Chem. Rev.* **104** (2004) 3267.
- 5) T. Sasaki: *Polym. J.* **37** (2005) 797.
- 6) K. Meerholz, B. L. Volodin, Sandalphon, B. Kippelen, and N. Peyghambarian: *Nature* **371** (1994) 497.
- 7) B. Kippelen and N. Peyghambarian: *Advances in Polymer Science, Polymers for Photonics Applications II* (Springer, Heidelberg, 2002) p. 87.
- 8) S. Tay, P.-A. Blanche, R. Voorakaranam, A. V. Tunç, W. Lin, S. Rokutanda, T. Gu, D. Flores, P. Wang, G. Li, P. St Hilaire, J. Thomas, R. A. Norwood, M. Yamamoto, and N. Peyghambarian: *Nature* **451** (2008) 694.
- 9) P.-A. Blanche, A. Bablumian, R. Voorakaranam, C. Christenson, W. Lin, T. Gu, D. Flores, P. Wang, W.-Y. Hsieh, M. Kathaperumal, B. Rachwal, O. Siddiqui, J. Thomas, R. A. Norwood, M. Yamamoto, and N. Peyghambarian: *Nature* **468** (2010) 80.
- 10) I.-C. Khoo: *Liquid Crystals: Physical Properties and Non-linear Optical Phenomena* (Wiley, New York, 1995).
- 11) H. Ono and N. Kawatsuki: *J. Appl. Phys.* **85** (1999) 2482.
- 12) G. P. Wiederrecht, B. A. Yoon, and M. R. Wasielewski: *Adv. Mater.* **12** (2000) 1533.
- 13) T. Sasaki, Y. Kino, M. Shibata, N. Mizusaki, A. Katsuragi, Y. Ishikawa, and T. Yoshimi: *Appl. Phys. Lett.* **78** (2001) 4112.
- 14) K. Skarp and M. A. Handschy: *Mol. Cryst. Liq. Cryst.* **165** (1988) 439.
- 15) P. Oswald and P. Pieranski: *Smectic and Columnar Liquid Crystals* (Taylor & Francis, New York, 2006).
- 16) T. Sasaki, A. Katsuragi, O. Mochizuki, and Y. Nakazawa: *J. Phys. Chem. B* **107** (2003) 7659.
- 17) T. Sasaki, O. Mochizuki, K. Noborio, and Y. Nakazawa: *J. Phys. Chem. B* **108** (2004) 17083.
- 18) M. Talarico, R. Termine, P. Prus, G. Barberio, D. Pucci, M. Ghedini, and A. Golemme: *Mol. Cryst. Liq. Cryst.* **429** (2005) 65.
- 19) M. Talarico and A. Golemme: *Nat. Mater.* **5** (2006) 185.
- 20) T. Sasaki, O. Mochizuki, Y. Nakazawa, G. Fukunaga, T. Nakamura, and K. Noborio: *Appl. Phys. Lett.* **85** (2004) 1329.
- 21) T. Sasaki, N. Moriya, and Y. Iwasaki: *J. Phys. Chem. C* **111** (2007) 17646.
- 22) T. Sasaki, D. Miyazaki, K. Akaike, M. Ikegami, and Y. Naka: *J. Mater. Chem.* **21** (2011) 8678.
- 23) T. Sasaki, M. Ikegami, T. Abe, D. Miyazaki, S. Kajikawa, and Y. Naka: *Appl. Phys. Lett.* **102** (2013) 063306.